Neural Network Modeling of Air Spring Dynamic Stiffness Based on Its Pneumatic Physics

Yuelian Wang , Bo Tao , Wenzheng Hu , Jiaqi Zhao , Fa Su , Zuguo Ma , Ye Zhuang *

Posted Date: 6 February 2026

doi: 10.20944/preprints202602.0491.v1

Keywords: air spring; nonlinear modeling; machine learning; physics-informed neural networks

 doi:10.20944/preprints202602.0491.v1

Article

Neural Network Modeling of Air Spring Dynamic Stiffness Based on Its Pneumatic Physics

Yuelian Wang [1], Bo Tao [2], Wenzheng Hu [3], Jiaqi Zhao [1], Fa Su [1], Zuguo Ma [4] and Ye Zhuang [1,*]

[1] National Key Laboratory of Automotive Chassis Integration and Bionics, Jilin University, No. 5988 Renmin Street, Changchun 130022

[2] Changchun Polytechnic University,No. 3278 Weixing Road, Economic and Technological Development Zone, Changchun City

[3] LinYi No.4 High School In ShanDong Province, Shandong Huaai Xingyao Power Techonogy Co., Ltd.

[4] Ningbo ZEEKR Automotive Research & Development Co., Ltd., No. 918, Binhai 4th Road, Hangzhou Bay New District, Ningbo, Zhejiang, 315336,P.R.China

* Correspondence: zhuangye@jlu.edu.cn; Tel.: +186-86522112

Abstract

To meet the real-time computational requirements of active suspension control systems, this study shifts from complex microscopic physical equations to a direct nonlinear functional mapping between the relative motion states (displacement and velocity) and the output force of air springs. This approach aims to preserve critical nonlinear hysteresis characteristics while significantly reducing the computational overhead. A progressive modeling strategy is implemented to characterize these complex behaviors. Initially, polynomial fitting is employed to identify key input features; however, its limited capacity to capture intricate nonlinearities necessitates more advanced methods. Subsequently, standard Feedforward Neural Networks (FNN) are explored for their nonlinear mapping capabilities, yet their inherent "black-box" nature often leads to convergence difficulties and restricted generalization. To address these issues, a Physics-Informed Neural Network (PINN) architecture is introduced, embedding physical governing equations as regularization constraints within the loss function to integrate data-driven flexibility with mathematical rigor. Recognizing that conventional PINNs often encounter convergence challenges due to conflicts between PDE constraints and data-driven loss terms, this research develops a Physics-Embedded Hierarchical Network (PEHN). By deriving specialized PDE constraints tailored to air spring dynamics and designing a hierarchical architecture aligned with these physical requirements, the PEHN effectively balances physical priors with experimental data. Experimental results demonstrate that the proposed PEHN ensures robust convergence and superior accuracy in capturing complex nonlinearities, hysteresis effects, and dynamic stiffness variations compared to baseline models.

Keywords: air spring; nonlinear modeling; machine learning; physics-informed neural networks

1. Introduction

As a critical component of modern automotive suspension systems, air springs play a pivotal role in enhancing ride comfort and handling stability, owing to their superior vibration isolation, adjustable stiffness, and height control capabilities. In contrast to traditional coil springs, the mechanical properties of air springs exhibit significant nonlinearity. This unique mechanical behavior affords them greater dynamic adaptability within active or semi-active suspension systems, allowing for adjustments based on varying driving conditions to optimize overall vehicle performance [1].

In the development of active suspension control systems, establishing a high-precision dynamic model of the air spring is a fundamental prerequisite for achieving closed-loop control [2]. Recent research into control strategies has frequently employed parametric modeling based on macroscopic

 doi:10.20944/preprints202602.0491.v1

characteristics. By establishing a functional mapping between the output force and the relative motion parameters of the sprung and unsprung masses [3], this method effectively characterizes the system's dynamic properties. Compared with first-principles physical modeling derived from gas equations of state, this data-driven parametric method accurately captures nonlinear hysteresis and dynamic stiffness variations [4], while simultaneously avoiding the heavy computational burden associated with complex fluid-structure interaction modeling.

Relevant research has been conducted on the characteristic modeling of air springs. Wu et al. [5] integrated thermodynamics and structural dynamics to develop a general model for dual-chamber air springs, elucidating the physical mechanisms behind stiffness and damping terms, particularly their frequency dependence. To address simulation complexities, Li et al. [6] employed fluid-structure interaction (FSI) modeling, revealing a significant performance asymmetry where axial compression proves more sensitive than tension due to radial load coupling. Further, Zhu et al. [7] proposed a high-fidelity model incorporating variable Berg friction and fractional derivatives. Unlike traditional linear models, their approach excels under large-amplitude excitations by capturing nonlinear elasticity and asymmetric hysteresis. Similarly, Chen et al. [8] introduced the TH-RCPPM model, utilizing RC operators to resolve the "bending effects" in hysteresis loops. Their experimental results confirmed high predictive accuracy, with dynamic relative errors below 7.1% even under complex conditions.

Although the aforementioned studies have significantly enhanced the physical fidelity and prediction accuracy of air spring models by incorporating thermodynamics, fluid–structure interaction, and fractional derivative theories, these models generally suffer from complex mathematical structures, challenging parameter identification, and high computational resource consumption. From the perspective of practical control strategy application, control systems prioritize the model's real-time computational efficiency and feasibility within the vehicle's onboard controller.

Consequently, instead of relying solely on complex microscopic physical equations, this study directly establishes a nonlinear functional mapping between the relative motion states (displacement and velocity) of the sprung and unsprung masses and the air spring output force. This approach aims to preserve the system's critical nonlinear hysteresis characteristics while significantly reducing the computational burden, thereby fulfilling the real-time requirements of active control systems.

In this study, a progressive modeling strategy is implemented to characterize the nonlinear behavior of air springs. Initially, polynomial fitting is employed not only to provide a preliminary representation but also to identify critical input features from the dataset. However, due to the limited capacity of polynomials in capturing intricate nonlinearities, standard Feedforward Neural Networks (FNN) [10] are subsequently explored. Although FNNs excel at nonlinear mapping, their inherent "black-box" nature often leads to convergence difficulties and restricted generalization. To overcome these limitations, a Physics-Informed Neural Network (PINN) [11] architecture is introduced. As a transformative paradigm in scientific computing, PINN has demonstrated exceptional robustness in solving complex nonlinear problems, even when faced with sparse or noisy data [12]. By embedding physical governing equations into the loss function as regularization constraints, the PINN model seamlessly integrates the flexibility of data-driven methods with the mathematical rigorousness of physical laws [9].

While Physics-Informed Neural Networks (PINNs) offer significant advantages, conventional PINN architectures often encounter convergence challenges [13]. Specifically, conflicts between PDE constraints and data-driven loss terms can arise, preventing the network from converging to the global optimum [14]. To address these limitations, this study refines the standard PINN framework by developing a Physics-Embedded Hierarchical Network (PEHN). By deriving specialized PDE constraints tailored to the dynamic characteristics of air springs and designing a hierarchical neural architecture aligned with these physical requirements [15], the PEHN effectively balances physical priors with experimental data. This approach ensures more robust convergence and a superior ability to capture complex behaviors, including nonlinearities, hysteresis effects, and dynamic stiffness

 doi:10.20944/preprints202602.0491.v1

variations. The resulting high-fidelity model not only accurately characterizes instantaneous mechanical responses but also provides a critical foundation for advanced suspension control strategies [16], such as Model Predictive Control (MPC), to enhance vehicle adaptability under dynamic loads. The overall research technical roadmap is illustrated in Figure 1, which details the evolutionary process from data acquisition to the proposed PEHN model.

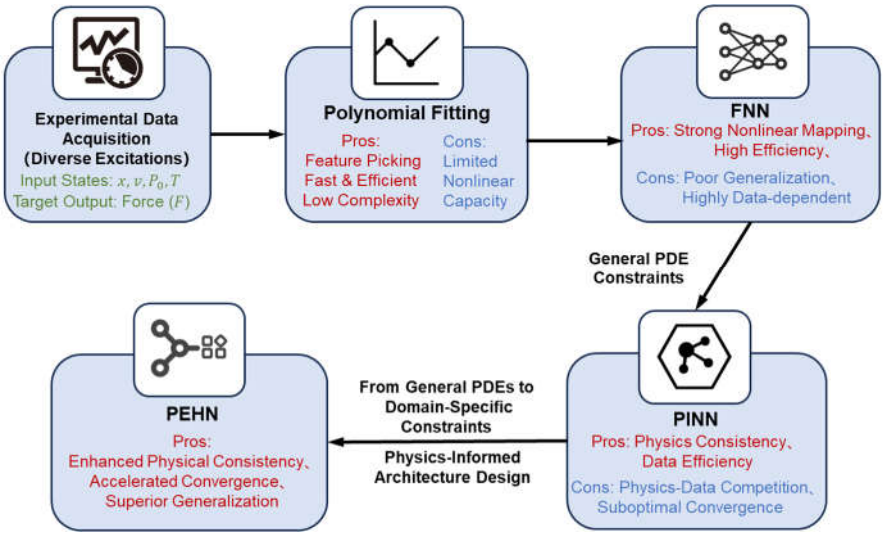

Figure 1. Proposed Technical Roadmap of Air Spring Nonlinear Modeling.

The main innovations of this paper are summarized as follows:1) Control-Oriented Characteristic Analysis: The external characteristics of the air spring are investigated from the perspective of control requirements. By utilizing the relative motion parameters between the sprung and unsprung masses as inputs, the output force of the air spring is directly obtained.2) High-Precision Surrogate Modeling: A Feedforward Neural Network (FNN) surrogate model is developed. This approach leverages the powerful nonlinear expression capability of neural networks to achieve higher precision in air spring modeling compared to traditional methods.3) Physics-Informed Neural Network Integration: A neural network model based on physical information is constructed. This integration accelerates the network's convergence speed and guides the model to converge in a direction consistent with physical laws, thereby significantly enhancing both prediction accuracy and generalization capability.

2. Experimental Study on External Characteristics of Air Springs

This research emphasizes the characterization of a system's physical behavior through empirical experimental data. High-quality experimental datasets regarding the external characteristics of air springs not only record mechanical responses under diverse operating conditions but also systematically reveal the inherent evolution of damping and stiffness variations [17]. Such data provides a robust foundation for establishing accurate mappings from operating states to mechanical performance. By leveraging these comprehensive datasets, the implemented modeling techniques—ranging from polynomial fitting for feature identification to neural networks for complex nonlinear capturing—can achieve high predictive accuracy while maintaining consistency with physical trends.

2.1. Preliminary Modeling of Air Springs

Assuming the air inside the air spring behaves as an ideal gas and the internal pressure is uniformly distributed, the external force F of the air spring can be expressed as:

$$F = (P - P_a)A_{eff}, \quad (1)$$

 doi:10.20944/preprints202602.0491.v1

where A_{eff} denotes the effective area of the air spring, P represents the pressure within the working volume, and P_a is the atmospheric pressure.

Air springs are suspension elements that use compressed air as an elastic medium, extensively used in automotive and high-speed railway applications. Operating on the principle of gas compressibility, the internal air generates an elastic force through compression or expansion under load. Therefore, the ideal gas polytropic equation is employed to describe the dynamic behavior of the air spring [18]:

$$P_0 V_0^r = const, \tag{2}$$

where P denotes the gas pressure and V denotes the gas volume, n is the polytropic exponent, determined by heat exchange conditions. Specifically, n = 1 corresponds to an isothermal process (characterized by slow change and sufficient heat exchange), while n = 1.4 corresponds to an adiabatic process (characterized by rapid change and no heat exchange). For other conditions, the value of n lies between 1 and 1.4.

The mechanical characteristics of an air spring exhibit pronounced nonlinear behavior, and the evolution of its internal gas state is essentially the result of the coupling between geometric deformation and thermodynamic processes. Specifically, the effective volume V of the air spring is not constant but varies nonlinearly with the relative displacement x between the sprung and unsprung masses. Meanwhile, the relative motion velocity v directly determines the rate of gas compression and expansion within the chamber, thereby influencing the degree of heat exchange between the gas and the surroundings, which in turn affects the polytropic index r and the evolution of transient internal pressure. Consequently, under dynamic operating conditions, both the working volume and the internal pressure should be formulated as dynamic functions of displacement and velocity, namely $V(x, v)$ and $P(x, v)$, so as to more accurately capture the mechanical response characteristics of the air spring [19].

Based on the aforementioned mechanism, it is necessary to establish a multi-physical quantity synchronous data acquisition system during the air spring external characteristic test. This system performs real-time measurement of key state variables during operation, including relative displacement x, relative velocity v, and internal pressure P. Furthermore, given that thermal effects during gas compression and expansion are non-negligible under actual working conditions, the real-time gas temperature within the chamber must be synchronously monitored. This allows for the correction of gas state deviations caused by temperature changes during the modeling process, thereby enhancing the physical consistency and reliability of the experimental data.

Simultaneously, according to the ideal gas polytropic equation, differences in state variables at the initial moment will affect the state of the entire model, namely:

$$P_0 V_0^r = P V^r, \tag{3}$$

Where P_0 represents the gas pressure at the initial state, and V_0 represents the initial volume of the gas within the air spring. The thermodynamic state of the system at the initial moment constitutes a critical boundary condition for the model. Specifically, the initial pressure P_0 and initial volume V_0 jointly determine the static equilibrium position and the fundamental stiffness characteristics of the air spring. Different initial states correspond to distinct stiffness evolution paths, thereby forming a family of mutually distinguishable stiffness curves. Therefore, during the testing process, the initial state parameters for each operating condition must be precisely calibrated and recorded. This ensures the accurate differentiation and unified modeling of various load levels and installation height conditions.

2.2. Test Rig Setup and Load Case Design

Guided by the aforementioned theoretical analysis and data acquisition requirements, a comprehensive experimental platform for characterizing air springs was established. This platform integrates mechanical excitation, pneumatic regulation, and high-frequency data acquisition

 doi:10.20944/preprints202602.0491.v1

capabilities, designed to precisely reproduce and observe the dynamic response of air springs under various operating conditions. The schematic diagram illustrating the overall control architecture and signal flow of the test rig is presented in Figure 1. As depicted, the testing system is primarily composed of three subsystems: the mechanical loading and execution unit, the pneumatic supply and regulation unit, and the real-time control and data acquisition unit (based on dSPACE). The specific hardware configurations and functions of these key subsystems are detailed as follows:

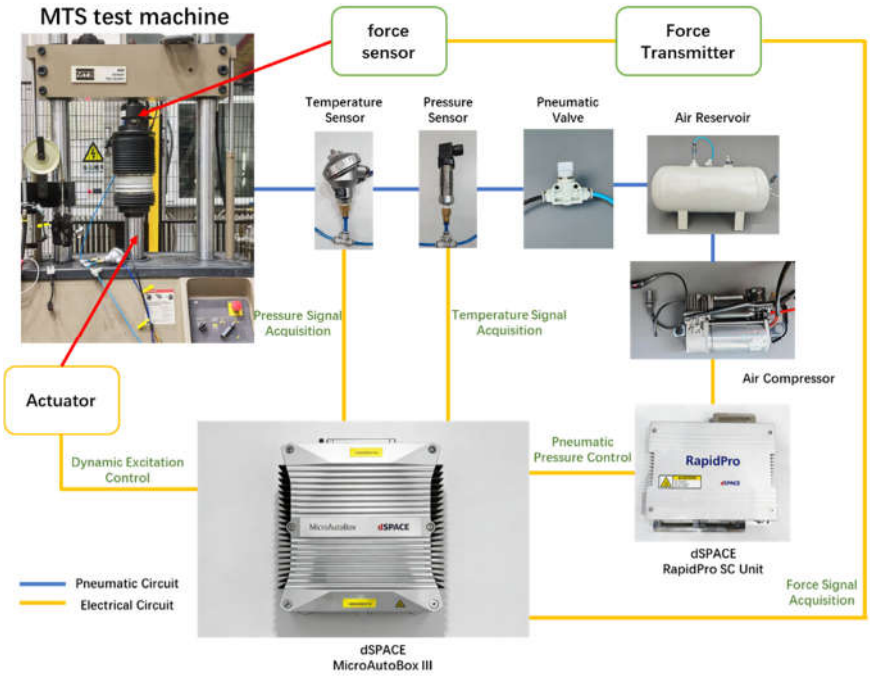

Figure 2. Schematic Diagram of the Testing Process for the External Characteristics of Air Springs.

MTS850 Damper Test System: To accurately investigate the mechanical properties of air springs under actual operating environments, this system is employed to apply preset loading excitations (including various typical input profiles) to the test specimen. During the loading process, integrated high-precision displacement sensors and velocity calculation modules capture the dynamic displacement response and velocity variation signals in real-time. Simultaneously, a force sensor located at the loading end synchronously acquires the instantaneous reaction force generated by the excitation. Through a multi-channel data acquisition system, the synchronized recording of displacement, velocity, and force signals is achieved, thereby obtaining the authentic dynamic response characteristics of the air spring under different loading conditions.

Air Spring:The specimen selected for this test is a double-chamber membrane air spring. Its design features a variable volume mechanism controlled by a solenoid valve. Specifically, when the solenoid valve is de-energized (normally open mode), the main and auxiliary chambers are connected, resulting in a total internal volume of $V = V_1 + V_2$. In this state, the air spring exhibits low stiffness, corresponding to the vehicle's Comfort Mode. Conversely, when the solenoid valve is energized, the valve port closes, isolating the passage between the two chambers. Consequently, the effective working volume is reduced to $V = V_1$. In this state, the air spring exhibits high stiffness, corresponding to the Sport Mode. Therefore, this experimental setup facilitates the acquisition of characteristic data for the air spring under two distinct initial volume configurations.

dSPACE MicroAutoBox III: The dSPACE MicroAutoBox III is a high-performance real-time control unit extensively utilized in Rapid Control Prototyping (RCP) and the testing of complex mechatronic systems. Serving as the core controller within this experimental platform, it is responsible for the centralized management and coordinated control of the entire test rig. Specifically, it generates precise excitation commands for the actuators based on preset operating conditions, ensuring that the dynamic characteristics of the mechanical loading process strictly adhere to

 doi:10.20944/preprints202602.0491.v1

experimental requirements. Simultaneously, through real-time closed-loop monitoring of the internal pressure within the air tank and air spring, it precisely regulates the solenoid valves and pneumatic supply equipment. This achieves both steady-state pressure maintenance and dynamic response regulation, thereby guaranteeing the stability and consistency of the system's operational state.

Beyond its core control capabilities, the MicroAutoBox III features robust multi-channel high-speed data acquisition functions, enabling the real-time capture, processing, and synchronized recording of key sensor signals such as pressure, displacement, and load, thus providing a reliable basis for subsequent data analysis. Additionally, the controller integrates comprehensive safety monitoring logic, capable of immediately triggering protective measures, such as emergency stops or pressure relief, upon detecting system anomalies to prevent equipment damage or safety incidents. In summary, the MicroAutoBox III deeply integrates control decision-making, signal coordination, and data management functions within this system, serving as the pivotal equipment for achieving high-precision air spring characterization tests.

dSPACE RapidPro SC Unit: The dSPACE RapidPro SC Unit is a specialized signal conditioning and power stage unit within the dSPACE modular platform. It possesses robust signal processing capabilities, enabling high-precision amplification, filtering, isolation, and excitation supply for sensor signals, as well as interface matching and power adaptation for actuator drive signals. Designed to operate seamlessly with the MicroAutoBox III, it establishes a high-precision, low-noise, and stable signal link for real-time control systems. In this experimental platform, the RapidPro unit primarily functions as the physical layer interface: it is responsible for level shifting or power amplification of the logic signals originating from the core controller. This provides compatible input interfaces for solenoid valves, pneumatic components, and actuators, thereby ensuring the precision and responsiveness of the actuation system.

Pressure Sensors: Pressure sensors in this system are primarily responsible for full-process pneumatic monitoring. During the preparation and inflation phase, these sensors perform real-time closed-loop monitoring of the internal pressure within both the air spring and the reservoir, ensuring that the system precisely and stably reaches the target pressure settings. Throughout the dynamic testing phase, the sensors continuously acquire transient pressure response data from the air spring. This function serves a dual purpose: it allows for real-time monitoring to detect if pressure fluctuations deviate from the normal operating range (preventing over-pressure or under-pressure anomalies), and it records essential experimental data to support subsequent mechanical characteristic analysis and performance evaluation.

Temperature Sensors: Given that temperature variations exert a significant influence on the polytropic exponent of the gas, thereby altering the mechanical properties of the air spring, this system is equipped with temperature sensors to perform real-time monitoring of the internal gas temperature. This measurement is critical for data reliability; it ensures the precise acquisition of key thermodynamic parameters during the testing process and provides the necessary physical basis for subsequent effective correction of thermal effects.

Pneumatic Valves: During the testing process, sensors are installed on the external pneumatic circuit for parameter measurement. To minimize the influence of the external circuit's volume on the effective working volume of the air spring, pneumatic valves (cutoff valves) are strategically positioned within the circuit. These valves are employed to reliably isolate the air spring from the upstream air supply (air reservoir) during measurement phases. This isolation effectively eliminates the interference of additional gas volume (dead volume) on the experimental results, thereby ensuring the physical fidelity of the test data.

Air Reservoir: The air reservoir plays a critical role in the air spring system, functioning as both a pressure stabilizer and a buffer. Firstly, acting as an intermediate energy storage element, it provides a sufficient and stable supply of compressed air to the air spring, effectively isolating the test object from pressure fluctuations originating from the upstream source (e.g., the compressor). Secondly, during inflation and deflation regulation, the reservoir buffers airflow variations, significantly dampening pressure pulsations and enhancing the system's dynamic stability and

 doi:10.20944/preprints202602.0491.v1

control precision. Furthermore, the stored pneumatic energy facilitates the rapid establishment of the air spring's initial operating pressure, ensuring the efficient and reliable execution of test conditions.

The design of the test conditions aims to comprehensively cover both typical and limit operating states of the air spring [20]. The excitation inputs are primarily categorized into steady-state sinusoidal excitation and transient random road input, which are used to characterize the system's dynamic response properties under periodic vibrations and random perturbations, respectively. Furthermore, by varying the initial pressure, initial compression (height), and working volume, a series of representative initial conditions were constructed. This allows for a systematic investigation of the mechanical performance and response characteristics of the air spring under different pre-charge states and dynamic deformation conditions [21].

Considering actual vehicle operating scenarios, air suspensions achieve functional differentiation through the synergistic regulation of height, pressure, and stiffness. Under the premise of a constant sprung mass, the correlation between common driving modes and the air spring state is as follows:

- Comfort Mode: Raises the vehicle body while maintaining lower pressure, utilizing the softening characteristics of the spring in its extended state to prioritize vibration isolation.
- Sport Mode: Lowers the vehicle body and increases pressure, leveraging the stiffening characteristics of the compressed airbag to enhance handling response.
- Off-road Mode: Significantly raises the vehicle body while maintaining medium pressure, utilizing the long stroke to achieve progressive stiffness (soft initially, stiffening under load) to ensure traversability.

To accurately characterize these operating modes, the corresponding initial pressure and height parameters were recorded for each case. The detailed experimental data and settings are organized in Table 1 below.

Table 1. Test Condition Table.

Test ID	Initial Temperature (°C)	Initial Pressure (MPa)	Test Conditions
1	22.412	0.205	20 mm, 0.4 Hz Sine Wave
2	22.748	0.288	20 mm, 0.4 Hz Sine Wave
3	22.644	0.387	20 mm, 0.4 Hz Sine Wave
4	23.059	0.481	20 mm, 0.4 Hz Sine Wave
5	22.720	0.582	20 mm, 0.4 Hz Sine Wave
6	22.379	0.205	20mm，1Hz Sine Wave
7	22.766	0.289	20mm，1Hz Sine Wave
8	22.678	0.386	20mm，1Hz Sine Wave
9	23.059	0.483	20mm，1Hz Sine Wave
10	22.720	0.580	20mm，1Hz Sine Wave
11	22.562	0.205	20mm，2Hz Sine Wave
12	22.675	0.290	20mm，2Hz Sine Wave
13	22.818	0.385	20mm，2Hz Sine Wave
14	22.855	0.485	20mm，2Hz Sine Wave
15	22.971	0.579	20mm，2Hz Sine Wave
16	22.171	0.196	Class A Random Road Profile
17	22.400	0.293	Class A Random Road Profile
18	22.504	0.390	Class A Random Road Profile
19	22.669	0.490	Class A Random Road Profile
20	22.739	0.585	Class A Random Road Profile

The loading phase was strictly limited to a duration of one minute. Upon achieving a steady state, continuous data were acquired for a period of 40 seconds. Notably, gas temperature fluctuations within the air spring remained below 0.5%, rendering thermal effects negligible in the

 doi:10.20944/preprints202602.0491.v1

data analysis. Therefore, the experiment is treated as an isothermal process, with the polytropic index r determined as 1.

3. Polynomial Regression Model

Focusing on the correlation between the relative motion of sprung/unsprung masses and the air spring output force, this study analyzes data collected under specific experimental conditions: an internal pressure of 0.205 MPa and a sinusoidal excitation (amplitude: 20 mm; frequency: 0.4 Hz). The aim is to elucidate the dynamic characteristics governing the relationship between relative displacement and the air spring's force response.

Theoretical analysis reveals a strong correlation between the relative displacement (sprung vs. unsprung mass) and the air spring output force. Linear regression analysis yielded an R^2 value of 0.9902, suggesting that the model captures the overall trend with high precision. Nevertheless, limitations exist in the linear approach, specifically in its inability to account for hysteresis effects. Since hysteresis involves non-linear mechanical responses during the loading and unloading phases, it cannot be adequately characterized by a linear model. Therefore, to achieve a precise simulation of the dynamic coupling between relative displacement and output force, future modeling must incorporate non-linear approaches to address hysteresis and related non-linear phenomena.

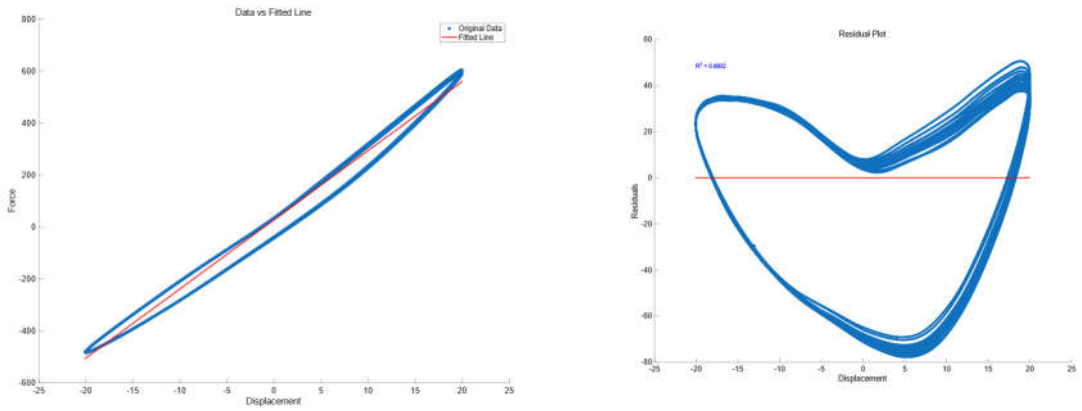

(**a**) (**b**)

Figure 3. (**a**) Linear Fitting of Air Spring Force-displacement Characteristics; (**b**) Residual Analysis of Linear Fitting Model.

To accurately model the hysteresis characteristics of the air spring, a velocity term was incorporated into the mechanical equation. The dynamic response of air springs—driven by internal gas compression/expansion and bladder deformation—is inherently rate-dependent. The inclusion of the velocity term allows for a more comprehensive representation of these dynamic effects [22].

While the model without the velocity term provided baseline predictions, it exhibited noticeable deviations and a low coefficient of determination (R^2), indicating limited fitting accuracy. Conversely, incorporating the velocity term significantly increased the R^2 value, demonstrating enhanced goodness of fit. This improved model not only precisely captures variations in output force but also effectively reproduces the hysteresis loop profile, resulting in a substantial reduction in overall residuals [23].

 doi:10.20944/preprints202602.0491.v1

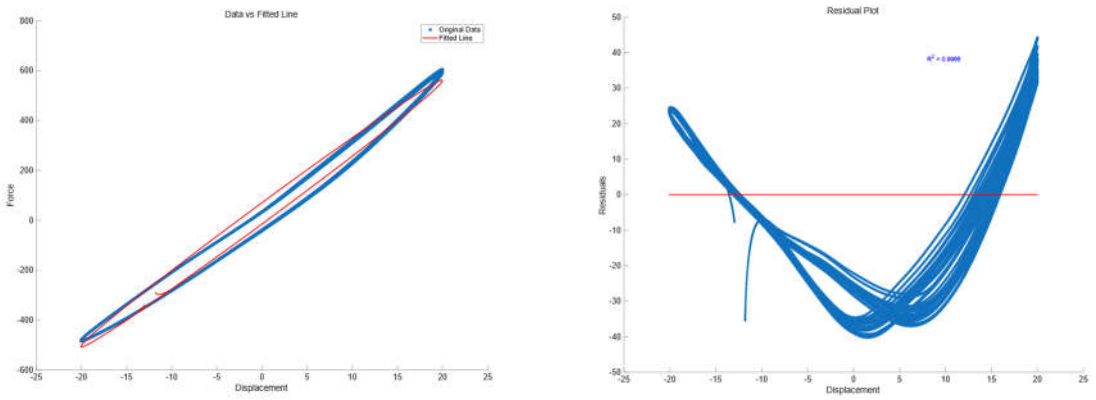

(**a**) (**b**)

Figure 4. (**a**) Linear Fitting Curve of Air Spring Based on Displacement and Velocity; (**b**) Residual Analysis of the Linear Fitting Model Based on Displacement and Velocity.

To enhance the predictive accuracy of the air spring mechanical model, this study incorporated a comprehensive set of second-order terms into the existing framework, specifically including additional quadratic and cross-product terms [24]. The results indicate that the coefficient of determination (R^2), a critical metric for assessing goodness of fit, improved significantly following the introduction of these terms. This enhancement demonstrates the model's increased explanatory power regarding data characteristics. Specifically, the model effectively captures a greater portion of the fluctuations in the dependent variable, thereby substantially elevating the overall fitting precision.

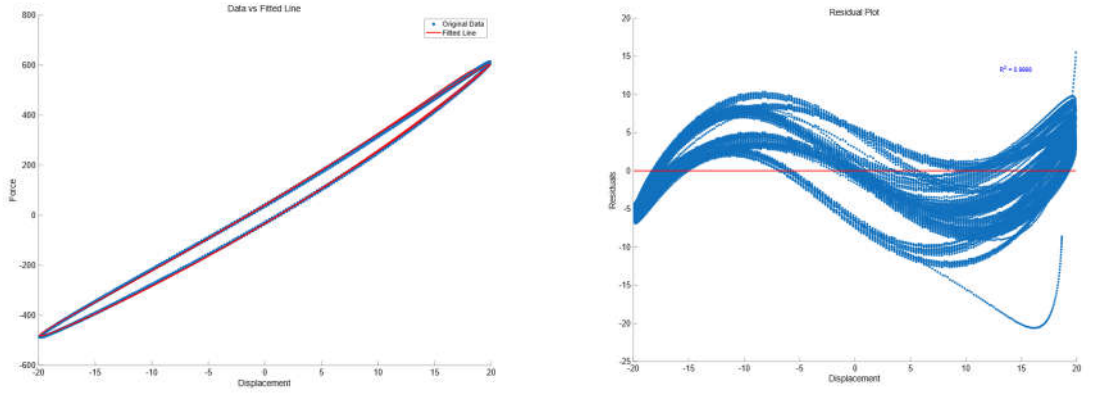

(**a**) (**b**)

Figure 5. (**a**) Second-order Regression Analysis of Air Spring Load-displacement-velocity Relationship; (**b**) Residual Analysis of the Second-order Fitting Model Based on Displacement and Velocity.

Based on the validation using multiple sets of measured data, a second-order fitting model incorporating the velocity squared term (v^2) and the displacement-velocity cross-product term ($x \cdot v$) was evaluated. The parameter estimation results indicate that the coefficients for these two terms are significantly smaller than those of the other terms. Given that the input variables are of the same order of magnitude, the influence of v^2 and v^2 was neglected. This approach simplifies the model while maintaining its fitting accuracy.

Table 2. Table of Coefficients for Quadratic Regression Model.

Terms	Constant term	x	v	x^2	v^2	$x \cdot v$
Weight	174	27.2411	0.1495	-0.2843	-0.0027	0.0000

 doi:10.20944/preprints202602.0491.v1

Guided by this analysis, the model was re-fitted after eliminating the velocity squared term and the displacement-velocity cross-product term. The results indicate no significant difference in fitting performance between the original and the simplified models. Comparative analysis of the force-displacement and force-velocity curves reveals that the predicted trajectories of both models track the measured data closely, exhibiting similar hysteresis characteristics. Furthermore, the distribution and magnitude range of the residuals remain consistent in both cases, demonstrating that the model's accuracy was not compromised.

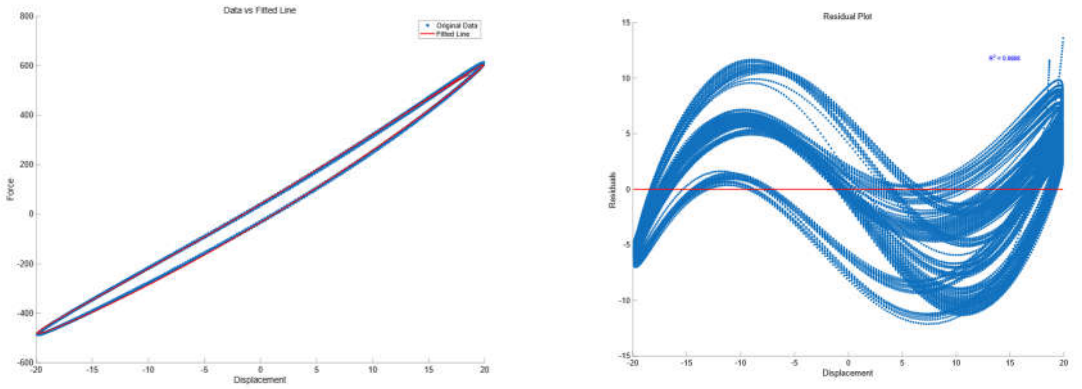

(**a**) (**b**)

Figure 6. (**a**) Optimized Displacement-velocity Quadratic Regression Model of Air Spring; (**b**) Residual Analysis of the Optimized Second-order displacement-velocity model.

Further validation of the model was conducted under multiple operating conditions. The results indicate that the calculated coefficient of determination (R^2) consistently remains at a high level, demonstrating the model's robust curve-fitting capability across different scenarios. However, it is worth noting that the fitting accuracy is relatively lower under random road excitation.

Table 3. Model Prediction Performance (R^2) by Operating Condition.

Working conditions	R^2
0.288MPa, 20mm, 0.4Hz Sine Wave	0.9995
0.289MPa, 20mm, 1Hz Sine Wave	0.9997
0.485MPa, 20mm, 1Hz Sine Wave	0.9997
0.196MPa, Class A Random Road Profile	0.9879
0.490MPa, Class A Random Road Profile	0.9852

In the study of air spring characteristics, dynamic performance varies significantly across different operating modes. Consequently, an accurate model must be capable of representing these various conditions by assigning specific fitting coefficients to each pressure level. However, when experimental data from varying initial pressures were input into a second-order polynomial model, the model failed to effectively distinguish between the pressure levels. This is because the fitting process prioritizes the minimization of global deviation, causing the result to converge toward a generic 'optimal' region while neglecting the subtle variations specific to each pressure condition. Although the model generates a reasonable curve for the aggregate data, its inability to differentiate the specific characteristics of individual initial pressures results in poor fidelity for specific conditions, thereby limiting its practical application in air spring analysis.

 doi:10.20944/preprints202602.0491.v1

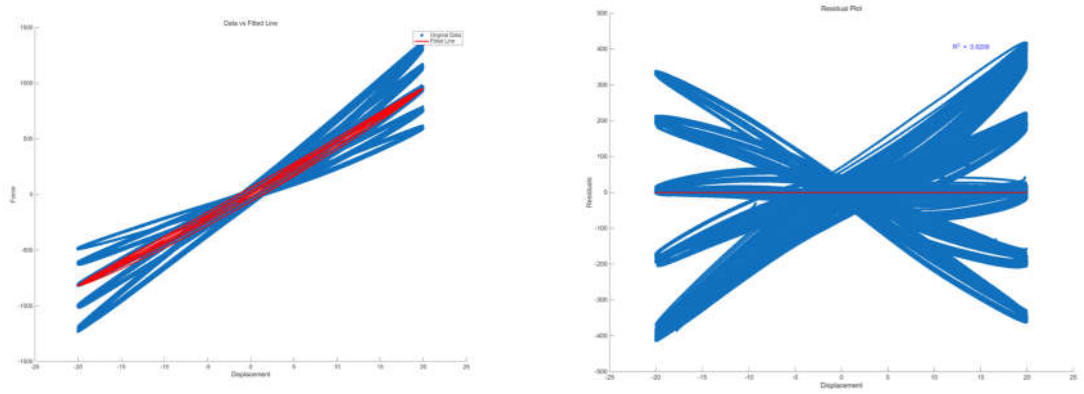

(**a**) (**b**)

Figure 7. (**a**) Second-order Optimized Regression Fitting of Air Spring under Multi-operating Conditions; (**b**) Residual Analysis of the Optimized Second-order Model under Multi-operating Condition.

To develop an air spring model capable of adapting to various operating modes while satisfying control requirements, distinct working modes were defined. Recognizing that each mode corresponds to a specific initial pressure (P_0), this parameter was incorporated into the model [25]. By combining P_0 with parameters describing the relative motion between the sprung and unsprung masses, a spring force model applicable to different operating conditions was formulated. The results of the second-order polynomial fitting are presented below:

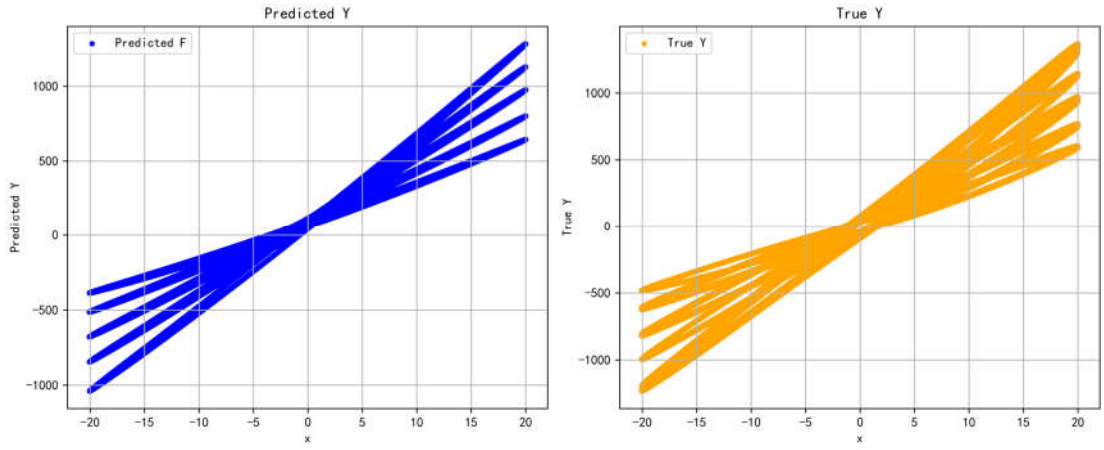

Figure 8. Multi-condition Fitting Characteristics of Air Spring Incorporating Initial Pressure Parameter.

An independent dataset under sinusoidal excitation was selected to validate the model. Since this validation set differs significantly from the training data in both excitation form and spectral characteristics, it provides a more authentic assessment of the model's adaptability and robustness under varying operating conditions. The validation results indicate that the model maintains high predictive accuracy under sinusoidal input, with a coefficient of determination (R^2) of 0.9748. This demonstrates the model's strong predictive capability and its effectiveness in characterizing the dynamic response of air springs under different excitation modes.

To further systematically evaluate the model's generalization performance, data derived from random road excitation under various initial pressures was utilized as the training set. Random road excitation simulates the response of air springs in actual operating scenarios and possesses high practical representativeness, thereby effectively capturing behavioral characteristics across multiple conditions. Consequently, the model exhibited excellent performance on this training set, achieving an R^2 of 0.9137, which highlights its strong fitting capability on the training data.

 doi:10.20944/preprints202602.0491.v1

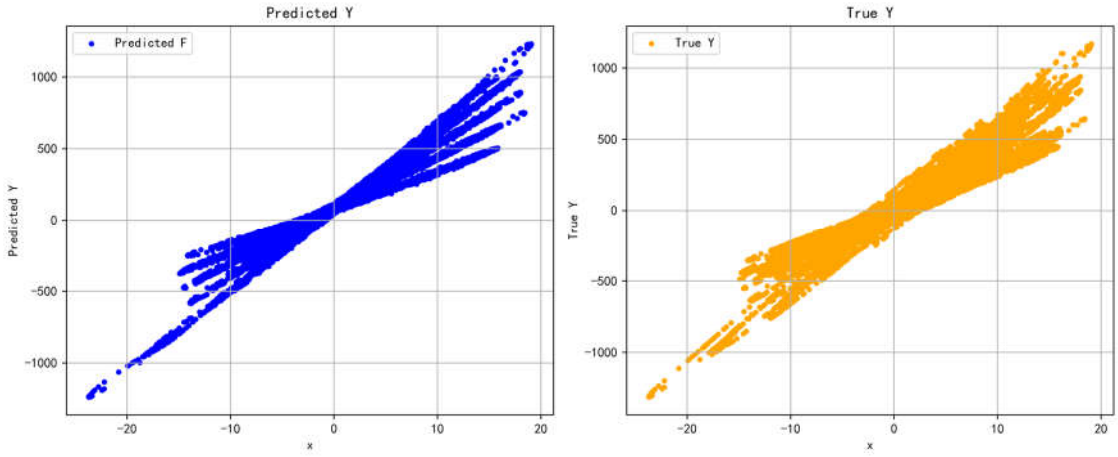

Figure 9. Response Fitting of Air Spring under Random Road Excitation and Varying Pressures.

However, under random road excitation, the input signal exhibits a broader frequency range and complex time-varying characteristics, significantly increasing the dimensionality of the system response. Constrained by its inherent structural limitations, the pure polynomial-based model struggles to fully characterize these strong nonlinearities and complex coupling behaviors. Consequently, for complex scenarios such as random excitation, it is necessary to introduce nonlinear modeling methods with more flexible architectures and stronger expressive capabilities to further enhance the prediction of complex system behaviors.

To intuitively evaluate the prediction error, the predicted data was compared with the measured data under a single sinusoidal operating condition, and the residuals were calculated. Given the periodic nature of the sinusoidal excitation, a 5-second segment of the data was extracted for observation, as shown in the figure below:

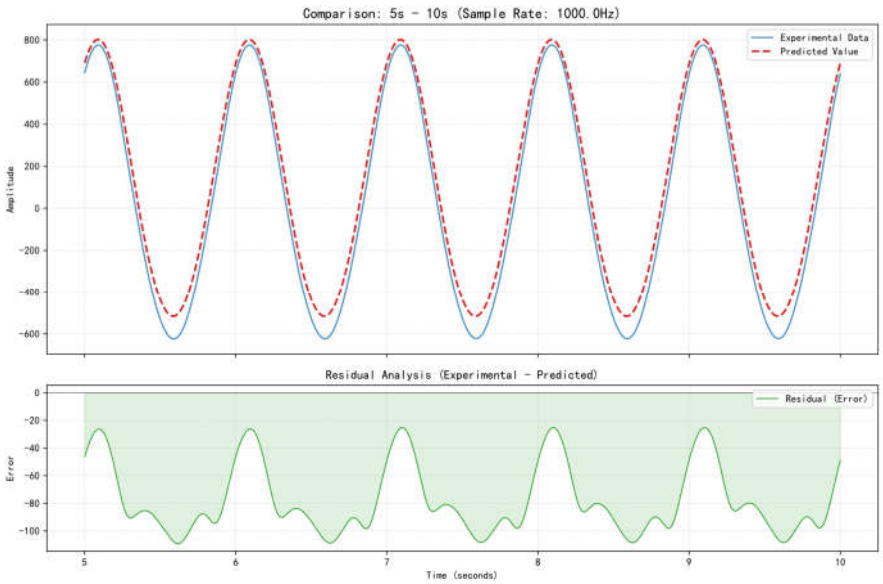

Figure 10. Time-domain Response Details and Deviation Analysis of Model Predictions.

It can be observed that while the polynomial model effectively captures the overall trend of the curve, it fails to fully represent certain nonlinear characteristics, resulting in some prediction deviations. Nevertheless, the fitting performance demonstrates that using initial pressure (P_0), relative displacement (x), and relative velocity (v) as input variables is sufficient to characterize the dynamic properties of the air spring under various operating conditions.

 doi:10.20944/preprints202602.0491.v1

4. Feedforward Neural Network

When employing polynomial fitting methods, it is often difficult to fully characterize the inherent non-linear properties of air springs due to the structural limitations of polynomial functions. particularly under multiple operating conditions, polynomial models struggle to capture the complex dynamic behaviors of air springs, resulting in limited fitting capability. Furthermore, from the perspective of physical mechanisms, the dynamic characteristics of an air spring involve complex interactions among the initial pressure P_0, the relative displacement between the sprung and unsprung masses x, and the relative velocity v [26]. These relationships are not only highly non-linear but also possess mathematical forms that are difficult to accurately describe using simple polynomial functions.

Given the limitations of polynomial fitting in addressing complex non-linear problems, this paper proposes the use of neural networks for air spring modeling. Neural networks possess strong non-linear approximation capabilities, allowing them to automatically learn complex mappings between inputs and outputs. They demonstrate superior performance, particularly in modeling high-dimensional features and non-linear systems. By leveraging neural networks, the model can extract features and characterize the non-linear dynamic behavior of air springs directly from extensive experimental data without relying on explicit analytical forms, thereby effectively overcoming the deficiencies of polynomial methods.

Consequently, neural networks not only effectively characterize the complex non-linear properties of air springs but also demonstrate robust generalization capabilities under varying operating conditions, rendering them an ideal approach for modeling dynamic behaviors. Through network training and optimization, the model can accurately predict air spring responses across different conditions, thereby significantly enhancing prediction accuracy and engineering applicability.

The Feedforward Neural Network (FNN) is a typical multi-layer neural architecture sequentially composed of an input layer, one or more hidden layers, and an output layer. Its defining characteristic is that information propagates solely in the forward direction, layer by layer, without any feedback loops. Specifically, the input layer receives the requisite system state variables and excitation inputs for modeling and transmits them to the hidden layers via weighted connections. Neurons in the hidden layers perform a linear weighted summation of the input signals, followed by a non-linear activation function to capture and map the system's non-linear characteristics. Finally, the output layer processes the features extracted by the hidden layers to generate predictions for the air spring's external characteristics or dynamic responses [27]. The overall architecture of the network is illustrated in the figure, where information transmission is achieved through fully connected layers.

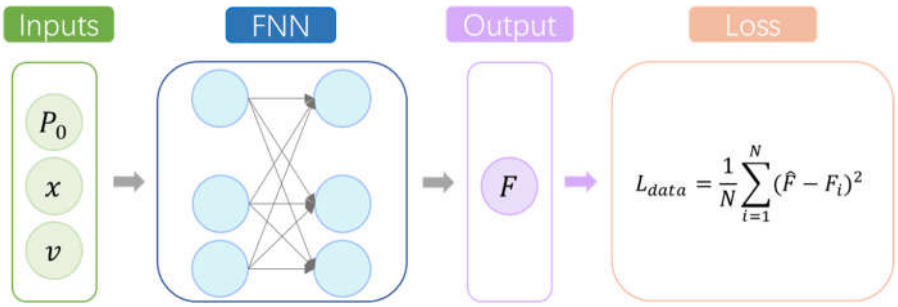

Figure 11. Architecture Diagram of the Feedforward Neural Network.

The output of an individual neuron is governed by the following formulation. The process initiates with a linear weighted summation of the input signals and their corresponding connection weights, followed by the addition of a bias term. Subsequently, a non-linear mapping is introduced

 doi:10.20944/preprints202602.0491.v1

via an activation function to yield the final neuronal output. The mathematical expression is given by [28]:

$$a_j = f\left(\sum_{i=1}^{n} w_{ij}\, x_i + b_j\right), \tag{4}$$

Where a_j denotes the output of the current neuron, x_i represents the output from the i-th neuron of the previous layer (acting as the input), w_{ij} signifies the connection weight between the i-th input and the j-th neuron, b_j is the bias term, and $f(\cdot)$ represents the non-linear activation function.

This study establishes a Feedforward Neural Network (FNN) learning model, with the network topology illustrated in the figure above. The input vector consists of three key variables: the initial pressure P_0, the relative displacement between the sprung and unsprung masses x, and the relative velocity v. The output corresponds to the resultant air spring force F. The combination of hidden layers and activation layers enables the effective characterization of the system's complex non-linear properties.

The specific network architecture was determined through extensive comparative simulations. A structure comprising two hidden layers was selected, with each layer containing 128 neurons. Experimental results indicate that further increasing the depth of the network yields no significant improvement in prediction performance. Consequently, the chosen configuration—finalized through iterative tuning—ensures high prediction accuracy while minimizing network complexity, thereby achieving a balance between model complexity and computational accuracy [29].

In addition, this study conducted a comparative evaluation of various activation functions, including Sigmoid, Tanh, and ReLU. Ultimately, ReLU was selected as the activation function. Comparative simulations indicate that, relative to other candidates, ReLU significantly accelerates network convergence and demonstrates superior convergence performance, characterized by lower training errors and higher stability.

$$ReLU(x) = \max(0, x), \tag{5}$$

For random road excitation conditions, the Feedforward Neural Network (FNN) demonstrates effective fitting capabilities, with the final prediction results illustrated in the figure above. The results indicate that the network has successfully captured the dynamic characteristics of the air spring and can accurately characterize its behavior under varying pressures. Specifically, the coefficient of determination (R^2) on the training set reached 0.9827. Compared to the second-order polynomial fitting model, the FNN achieves a relative improvement in prediction accuracy, demonstrating distinct advantages in both feature extraction and non-linear representation capabilities.

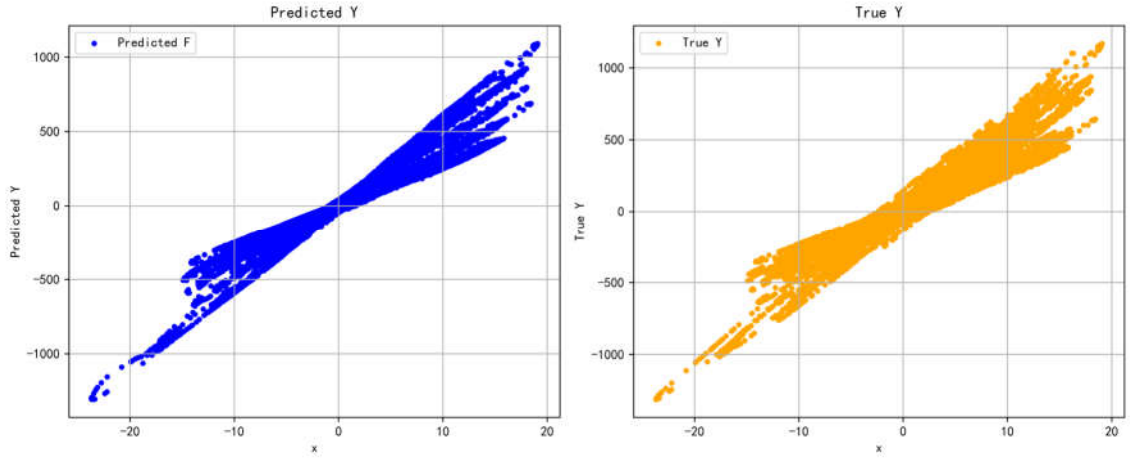

Figure 12. Prediction Validation of the Feedforward Neural Network under Stochastic Road Excitation.

To evaluate the generalization capability of the Feedforward Neural Network (FNN) model, sinusoidal excitation conditions were selected as the test set. Characterized by their periodicity and

 doi:10.20944/preprints202602.0491.v1

regularity, sinusoidal conditions effectively simulate dynamic variations encountered in practical applications and serve to validate the network's prediction performance under varying frequency inputs. Upon applying the sinusoidal test set to the model, results indicated that the coefficient of determination (R^2) reached 0.9870 on both the training and test sets. This high degree of accuracy demonstrates the model's superior performance in characterizing air spring behavior, indicating that the FNN has effectively captured the dynamic properties of the air spring across different initial pressures and excitation frequencies.

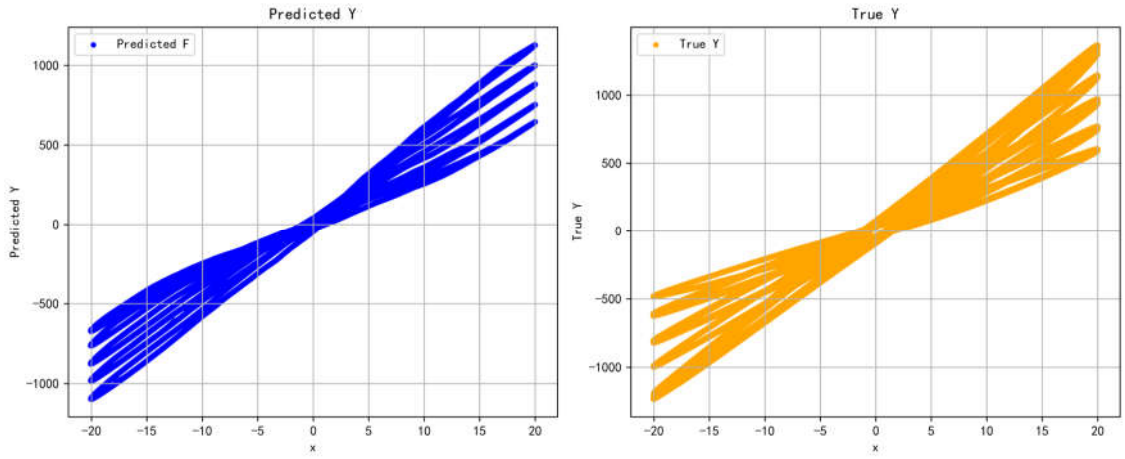

Figure 13. Prediction validation of the Feedforward Neural Network under Sinusoidal Excitation.

Compared with the polynomial fitting model, the Feedforward Neural Network (FNN) model demonstrates significant superiority across all evaluation metrics. Polynomial models rely on predetermined functional forms, and their representation capability is strictly constrained by the model order. Although acceptable fitting accuracy may be achieved under specific conditions (such as random road excitation), these models struggle to effectively characterize complex non-linear system behaviors when input features exceed the training data distribution or when unlearned excitation patterns are encountered, leading to a marked deterioration in prediction performance.

In contrast, the FNN model, leveraging its multi-layer non-linear architecture and adaptive learning mechanisms, is capable of automatically extracting and characterizing high-order features and latent patterns within the data. This results in a more comprehensive and accurate description of the system's non-linear characteristics.

To further quantify the model's performance, a detailed validation was conducted under typical sinusoidal operating conditions. By visualizing the alignment between the predicted and measured trajectories, the prediction deviations were intuitively characterized. Given the periodic nature of sinusoidal signals, a 5-second segment of representative time-domain data was randomly extracted for localized zoomed-in analysis. Simultaneously, the residual distribution was calculated to evaluate the model's transient tracking accuracy under dynamic loads.

 doi:10.20944/preprints202602.0491.v1

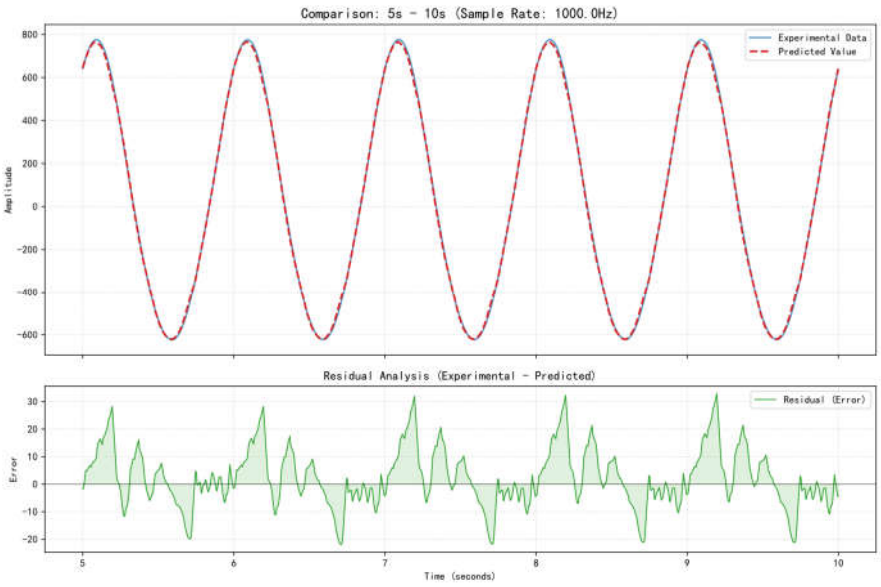

Figure 14. Time-domain Response and Deviation Analysis of the Feedforward Neural Network Model Predictions.

The neural network demonstrates superior capability in characterizing non-linear properties and captures the global trends of the model with greater precision. Simultaneously, prediction bias is significantly reduced, resulting in enhanced overall prediction accuracy.

Furthermore, the Feedforward Neural Network exhibits distinct advantages regarding generalization performance. Even under varying input conditions or in the presence of significant uncertainty, the model maintains high prediction accuracy and stability. This robust adaptability to complex and variable inputs renders it highly advantageous for practical engineering applications. In summary, the neural network model outperforms the polynomial fitting model in terms of prediction accuracy, non-linear representation capability, and generalization robustness. Therefore, it is significantly better suited for the modeling and prediction of complex dynamic systems, such as air springs, under multiple operating conditions.

5. Physics-Informed Neural Network

The Physics-Informed Neural Network (PINN) is an advanced framework that deeply integrates physical mechanism constraints with data-driven methodologies. The primary objective of introducing PINN in this study is to establish a "data-modeling dual-driven" strategy. Its core philosophy lies in explicitly embedding the system's physical laws into the neural network training process, thereby effectively constraining the solution space and enhancing learning efficiency. In the context of air spring dynamic modeling, traditional purely data-driven models typically rely heavily on extensive experimental data and are prone to generating physically inconsistent predictions under drastically varying conditions. In contrast, by incorporating the intrinsic physical characteristics of the air spring into the optimization objective, PINN not only addresses the limitations of purely data-driven approaches but also achieves a truly synergistic dual-drive of experimental data mining and physical modeling [30].

Specifically, PINN employs the neural network as a universal function approximator. While utilizing experimental data to learn the non-linear input-output mapping of the air spring, it explicitly embeds physical constraints governing the dynamic behavior—such as force-displacement-pressure constitutive relations, state evolution equations, or system conservation laws—into the loss function as penalty terms. Consequently, the model's training objective encompasses the minimization of both the fitting error regarding experimental data and the residuals derived from physical constraints.

 doi:10.20944/preprints202602.0491.v1

This mechanism effectively guides the optimization of network parameters, ensuring the learning process proceeds under the premise of physical consistency [31].

Moreover, the incorporation of physical information helps reduce the model's dependency on complex network architectures and extensive training datasets [32]. This enables PINN to demonstrate superior generalization capability and robustness in engineering systems like air springs, which are characterized by strong non-linearity, high parameter uncertainty, and variable operating conditions. Compared with traditional Feedforward Neural Networks, PINN typically achieves faster convergence rates and a more stable training process while maintaining modeling accuracy. This establishes a more reliable foundation for the real-time modeling and control applications of air springs in active suspension systems.

In view of the severe non-linearity and hysteresis associated with air springs, sole reliance on data fitting is frequently insufficient to satisfy stringent engineering precision standards. Consequently, this study incorporates a physical mechanism constraint framework, achieving a synergistic integration of the air spring's intrinsic physical properties—including effective area dynamics and gas state equations—within the computational model [33]. Governed by strict physical laws, the model exhibits enhanced convergence stability and higher fidelity in representing actual physical processes. Crucially, this physics-enhanced paradigm demonstrates robust generalization capabilities; it sustains stable performance even when encountering unseen datasets or extreme operating conditions, thus meeting the rigorous reliability requirements of practical engineering.

Current approaches to air spring modeling generally employ mechanistic analysis, seeking to formulate mathematical representations based on granular internal structural parameters—including bladder geometry, cord angles, and piston profiles. However, this parametric strategy is heavily contingent upon precise physical priors. When dealing with complex internal topologies or high degrees of geometric non-linearity, the derivation of accurate explicit analytical expressions proves to be a formidable, and often unachievable, task. Such theoretical intractability poses a significant impediment to the deployment and scalability of these methods within complex, next-generation structural designs.

Consequently, we propose to model the dynamic behavior of air springs by leveraging generalized theoretical equations integrated with the neural network's robust capacity for representing complex non-linear systems:

$$F = PA_{eff}, \tag{6}$$

Where P denotes the pressure difference between the internal and ambient pressures, and A_{eff} represents the effective working area of the air spring. Based on the strategy of modeling the dynamic characteristics of P and A_{eff}, the network architecture is constructed as illustrated in the figure below.

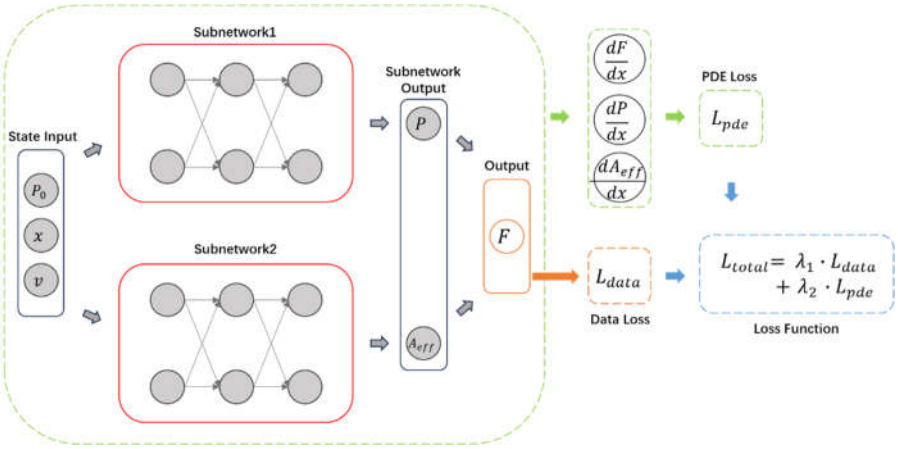

Figure 15. Architecture Diagram of the Physics-Informed Neural Network.

 doi:10.20944/preprints202602.0491.v1

Physical constraints are established to guide the convergence of the neural network using Partial Differential Equations (PDEs). As indicated by the aforementioned derivations, both P and A_{eff} are functions of the relative displacement x between the sprung and unsprung masses. Consequently, the PDE constraints that the neural network must satisfy are defined as follows:

$$\frac{dF}{dx} = \frac{dP}{dx}A_{eff} + P\frac{dA_{eff}}{dx}, \tag{7}$$

In order to achieve effective decoupling and precise extraction of the physical variables governed by PDE constraints, we introduce a physics-decoupled parallel neural network framework designed to resolve the complexities of modeling nonlinear strongly coupled systems. Guided by the system's underlying physical topology, the architecture partitions the modeling task into dual independent subspaces. Specifically, Sub-network 1 focuses on the identification of thermodynamic dynamics regarding chamber pressure (P), whereas Sub-network 2 operates in parallel to capture the time-varying geometric characteristics of the effective area (A_{eff}) [34]. These components are integrated via a physics-fusion layer, which rigorously applies mechanical constitutive laws to synthesize the final output force (F). This approach significantly reduces the complexity of high-dimensional surface fitting and, through explicit decoupling, imparts clear physical interpretability to the intermediate nodes of the network.

In order to guarantee robust generalization in data-limited regimes, we leverage the Physics-Informed Neural Network (PINN) framework to formulate a hybrid loss function that incorporates data fidelity alongside physics residuals. The dynamic stiffness PDE is integrated as a fundamental prior constraint within the optimization landscape, functioning as a physical regularizer that directs the training trajectory toward dynamically conserved solutions. By enforcing strict compliance with physical laws during error minimization, this approach maintains physical consistency even where data is scarce, thereby establishing a credible dynamic model with high precision and robustness. These constraints are unified within the loss function, where the minimization process serves to constrain the model's convergence, ensuring it satisfies:

$$L_{total} = \lambda_1 L_{data} + \lambda_2 L_{phy}, \tag{8}$$

In this formulation, λ_1 and λ_2 serve as the weighting factors for the data and physics terms. The selection of these weights is optimized based on the magnitude disparity between the loss functions and the model's convergence dynamics.

The proposed PINN achieves robust fitting performance under random road conditions. As shown in the figure, the network effectively characterizes the nonlinearity of the air spring and provides an accurate representation of its dynamics across different pressure levels. Furthermore, the model achieves a coefficient of determination (R^2) of 0.9767 on the training set. This demonstrates that the PINN maintains a prediction accuracy comparable to standard feedforward neural networks, while incorporating physical validity.

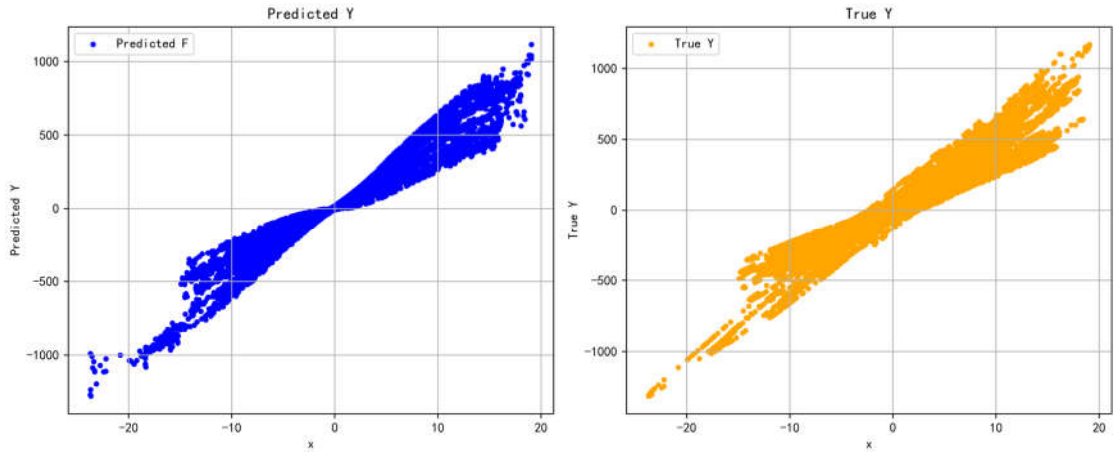

 doi:10.20944/preprints202602.0491.v1

Figure 16. Prediction validation of the Physics-Informed Neural Network (PINN) under stochastic road excitation.

To assess the generalization capability, the PINN model was evaluated using the same dataset under sinusoidal operating conditions. The results reveal that the coefficient of determination (R^2) remained consistent at 0.9748 for both the training and testing sets. Notably, the PINN exhibits a marginal performance deficit compared to the standard FNN. This is mainly due to the higher architectural complexity, where the requirement for the synchronous convergence of dual sub-networks—governed by strict physical constraints—imposes a greater burden on the optimization process, thereby slightly affecting the ultimate prediction precision.

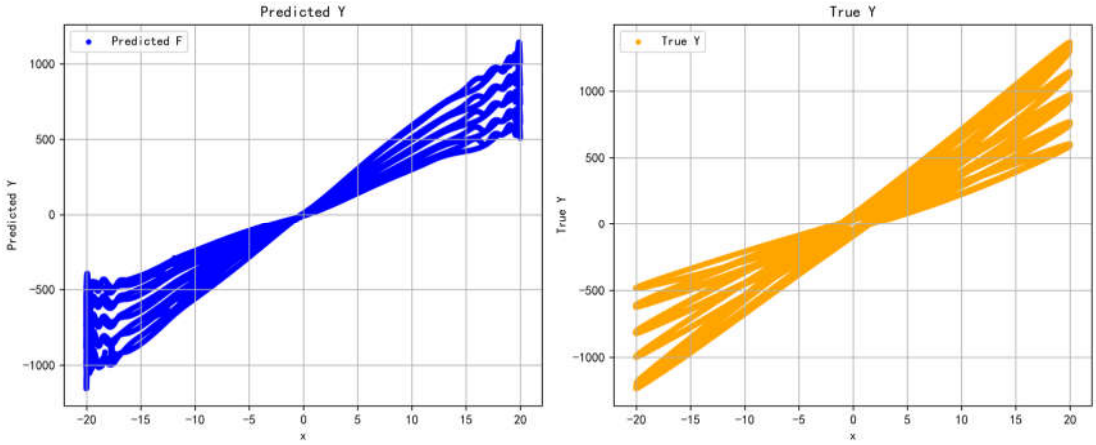

Figure 17. Comparison of PINN-based responses under sine inputs with varying frequencies.

We validated the nonlinear mapping capabilities and temporal stability of the model using typical sinusoidal load cases. As demonstrated by the time-domain response comparison, the predictions (red dashed line) align closely with the experimental measurements (blue solid line) in terms of phase and magnitude. The model successfully captures the periodic dynamics of the physical system without exhibiting obvious phase delays or amplitude decay.

A quantitative analysis of the residuals further confirms stability; the error sequence remains consistently confined within the ±100 bound during the 5s–10s interval, with no temporal divergence. Nevertheless, a critical observation is that the residuals display a clear harmonic oscillation pattern. This implies a structural discrepancy: although the physics constraints guarantee robustness, the current PDE does not perfectly capture the complex nonlinearities, thereby imposing a rigidity that hinders the network's convergence toward the global optimum. Therefore, resolving this trade-off necessitates the investigation of a more appropriate PDE constraint—one that is strictly tailored to the system's properties—to assist the neural network in achieving optimal convergence.

 doi:10.20944/preprints202602.0491.v1

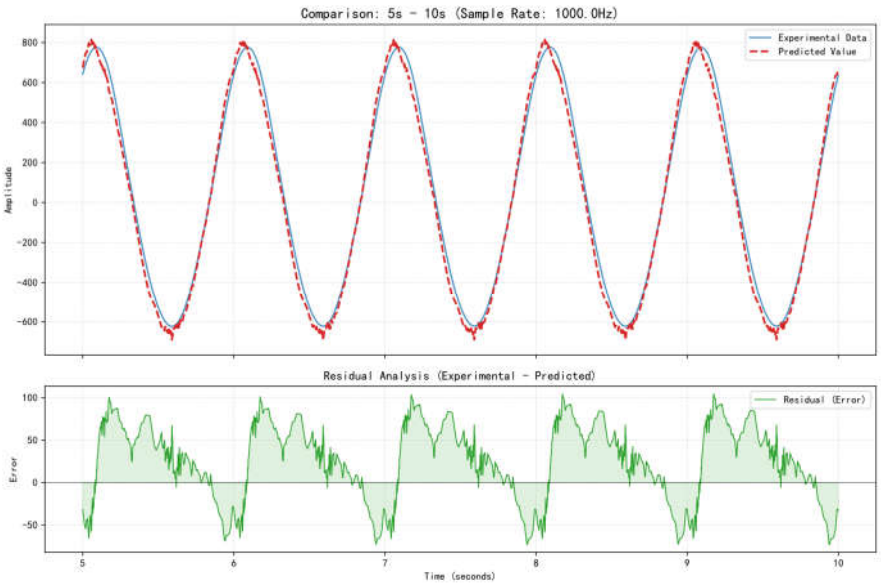

Figure 18. Time-domain Response Details and Residual Analysis of PINN under a Single Sinusoidal Condition.

We consider using a more specific PDE constraint equation to further link the neural network structure with the physical model. This imparts physical meaning to the network and helps the entire model converge synchronously, with the expectation of better learning results.

As the experiment operates under isothermal conditions, the gas equation of state indicates that the initial state meets the following condition:

$$P_0 V_0 = const, \tag{9}$$

By differentiating both sides of the equation, we obtain:

$$P_0 \frac{dV}{dx} + V_0 \frac{dP}{dx} = 0, \tag{10}$$

Therefore, we obtain:

$$\frac{dP}{dx} = -\frac{P_0}{V_0}\frac{dV}{dx}, \tag{11}$$

Thus, for the air spring starting from the initial state, we have:

$$\frac{dF}{dx} = -\frac{P_0}{V_0}\frac{dV}{dx}A_{eff0} + P_0\frac{dA_{eff}}{dx}, \tag{12}$$

When the compression displacement is infinitesimally small, we assume [35]:

$$dV \approx -A_{eff0}dx, \tag{13}$$

In this case, the dynamic stiffness formula becomes:

$$K_{dyn} = \frac{dF}{dx} = \frac{P_0}{V_0}{A_{eff0}}^2 + P_0\frac{dA_{eff}}{dx}, \tag{14}$$

After simplification, we obtain:

$$K_{dyn} = \frac{dF}{dx} = P_0\left(\frac{{A_{eff0}}^2}{V_0} + \frac{dA_{eff}}{dx}\right), \tag{15}$$

The initial state parameter $\frac{{A_{eff0}}^2}{V_0}$ is calculated using the experimental data. Subsequently, the dynamic stiffness formula is employed as a PDE constraint to facilitate the convergence of the neural network.

Given that the differential terms in the partial differential equation (PDE) explicitly involve the output force F and the effective area A_{eff}, and taking the mathematical structure of the formula

 doi:10.20944/preprints202602.0491.v1

into full account, this study reconstructs a physics-embedded cascaded neural network architecture. This architecture aims to enhance model interpretability by incorporating structured prior knowledge, while simultaneously attempting to address the issue of unsatisfactory convergence often encountered in PINN models.

The network adopts a hierarchical strategy for processing physical information: The first sub-network is designed to infer the intermediate physical quantity—chamber pressure (P)—from the initial state inputs. Subsequently, this critical intermediate variable is explicitly propagated to the second sub-network [36], where it undergoes deep feature fusion with the original motion states to finally resolve the system's output force (F) and effective area (A_{eff}) via nonlinear mapping.

This serial architecture accurately reconstructs the physical causality of the real system—where 'state determines pressure, while pressure and motion synergistically drive the output'—thereby significantly reducing the difficulty of fitting complex nonlinear dynamics.

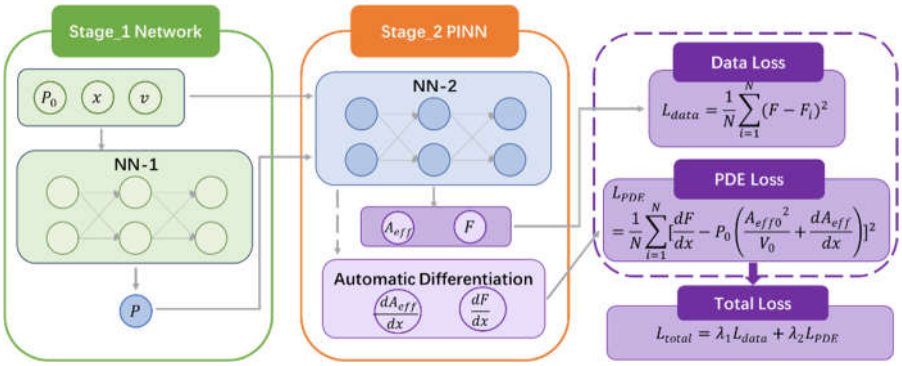

Figure 19. Architecture Diagram of the Physics-Embedded Hierarchical Network.

The Physics-Embedded Hierarchical Network (PEHN) demonstrates exceptional performance in handling random road excitations by combining the strengths of physical laws and data-driven approaches. As illustrated in the figure, the improved network effectively captures the dynamic characteristics of air springs under varying pressures. The model achieves a coefficient of determination (R^2) of 0.9839 on the training set, outperforming previous models in prediction accuracy. Crucially, the convergence speed is significantly enhanced: the model converges within just 1 to 2 epochs with the same dataset size. This improvement not only ensures high-precision prediction but also substantially reduces computational costs and training time.

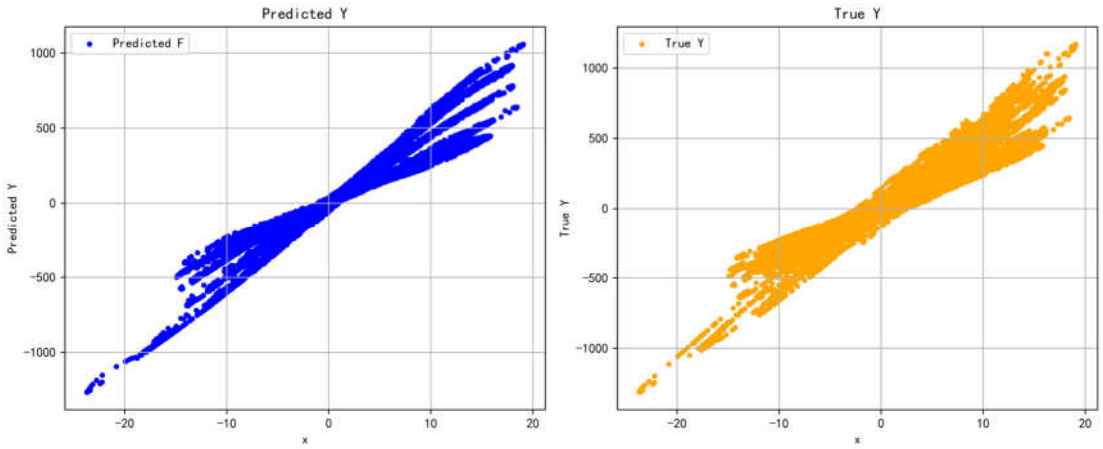

Figure 20. Prediction validation of the Physics-Embedded Hierarchical Network under multiple stochastic road profiles.

 doi:10.20944/preprints202602.0491.v1

Additionally, the model attains an R^2 of 0.9904 under sinusoidal testing conditions, outperforming previous models in comprehensive capabilities. This evidence reinforces the conclusion that the physics-embedded architecture possesses a distinct advantage in the precise representation of system nonlinearities.

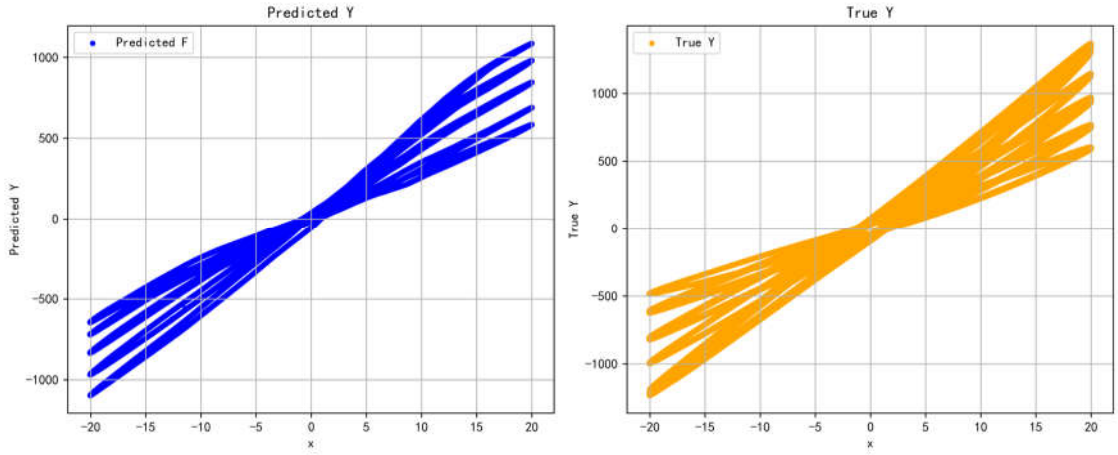

Figure 21. Prediction validation of the Physics-Embedded Hierarchical Network under sinusoidal excitation.

In this study, high-frequency dynamic tracking validation was conducted using a single sinusoidal operating condition. The time-domain comparison from 5s to 10s reveals a high degree of alignment between the predicted curve (red dashed line) and the experimental curve (blue solid line). The model achieves precise synchronization with zero phase lag, accurately capturing both the extremum values at peaks and valleys and the transient changes at zero-crossings.

Quantitative residual analysis further confirms the performance improvement. Compared to previous models, the residual range of the proposed model has significantly narrowed to the [-15, 25] interval. Given the signal amplitude of approximately 800 N, the relative error is maintained within 3%. The residual sequence fluctuates stably around zero without obvious outliers, conclusively demonstrating the model's excellent generalization capability and operational stability when processing unseen data.

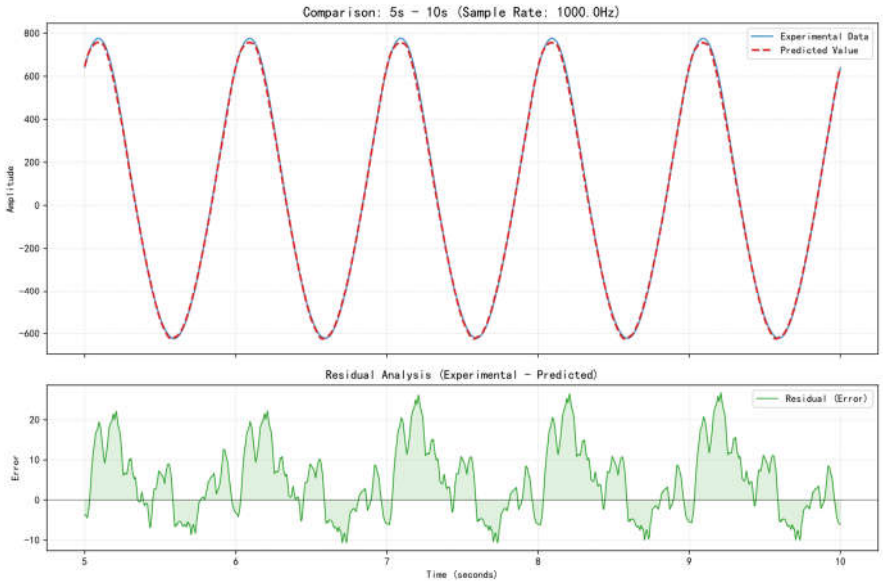

Figure 22. Time-domain response details and residual analysis of the Physics-Embedded Hierarchical Network under a single sinusoidal condition.

 doi:10.20944/preprints202602.0491.v1

As shown in Table 4, the physics-informed architecture demonstrates superior performance across both validation and test datasets. With R^2 values significantly outperforming other models, it achieves the highest overall level of prediction accuracy.

Table 4. Summary Table of Goodness-of-Fit Statistics (R^2)for Validation and Test Data.

Model	Validation Set R^2	Test Set R^2
Polynomial Regression Model	0.9137	0.9748
Feedforward Neural Network	0.9827	0.9870
Physics-Informed Neural Network	0.9767	0.9748
Physics-Embedded Hierarchical Network	0.9839	0.9904

As summarized in the table, the Physics-Informed Architecture Neural Network demonstrates the best overall performance among all compared models. While the Feedforward Neural Network (FNN) shows decent performance, the proposed model significantly enhances generalization capability by incorporating physical architectural constraints. Specifically, it achieves coefficients of determination (R^2) of 0.9839 on the validation set and 0.9904 on the test set, outperforming the polynomial fitting, traditional FNN, and standard PINN models. This strongly evidences the superiority and robustness of the hierarchical physics-embedded architecture in handling complex nonlinear mappings.

6. Conclusions

From the perspective of suspension control, this study focuses on predicting the air spring output force required for control purposes, using the relative motion parameters between the sprung and unsprung masses as inputs while minimizing modeling complexity. By constructing a physics-informed neural network architecture, the model effectively incorporates physical constraints into the data-driven process. This approach accelerates convergence, facilitates the extraction of nonlinear characteristics, and significantly enhances generalization capabilities. Future research will explore physical modeling methods for complex air spring structures, such as those with auxiliary chambers, to extend the model's applicability under extreme dynamic conditions. In summary, dynamic modeling and optimal control of air springs are key technologies for improving modern vehicle suspension performance, holding significant importance for the continuous optimization of ride comfort, safety, and handling.

The main achievements and conclusions are as follows:

- A second-order polynomial fitting model was established. Using the relative motion parameters between the sprung and unsprung masses as inputs, the model fits the output force. The comparison between simulation results and experimental data verified the validity of the model (the coefficient of determination, R^2, on the sinusoidal dataset reached 0.9748). Furthermore, by incorporating the initial pressure parameter, the model effectively characterizes the mechanical properties of the air spring under different working modes, providing a reliable baseline model for suspension control research;
- We developed and assessed a Feedforward Neural Network (FNN) model for air spring force prediction. The model's effectiveness was confirmed through training and testing, achieving R^2 values higher than 0.98 under both random excitation and sinusoidal operating conditions. Comparative results demonstrate that the FNN model exhibits superior overall performance and adaptability on the validation and test sets compared to the second-order polynomial fitting model;
- A neural network model based on a physics-informed architecture was constructed. By restructuring the network architecture according to general physical theories, the proposed method aims to guide the network convergence toward a manifold consistent with physical laws, subject to data constraints. This approach effectively enhances the convergence speed.

 doi:10.20944/preprints202602.0491.v1

Experimental results demonstrate that the physics-informed model achieves superior prediction accuracy on both validation and test sets compared to the second-order polynomial fitting model and the traditional feedforward neural network model.

Author Contributions: Conceptualization, Y.W.; methodology, Y.W. and Y.Z.; software, Y.W. ,J.Z. and F.S.; validation, Y.W.; formal analysis, Y.W.; investigation, Y.W.; resources, Y.W.; data curation, Y.W.,J.Z. and F.S.; writing—original draft preparation, Y.W..; writing—review and editing, Y.W.; visualization, Y.W. and Z.M.; supervision, Y.W., B.T., W.H. and Y.Z.; project administration, Y.W.; funding acquisition, Y.W., B.T., W.H. and Y.Z.; All authors have read and agreed to the published version of the manuscript.

Funding: This research was funded by the National Natural Science Foundation of China, grant number~ 52372386 and the Science and Technology Development Project of Jilin Province, grant number~202502007.

Data Availability Statement: No new data were created or analyzed in this study. Data sharing is not applicable to this article.

Acknowledgments: The authors would like to thank the anonymous referees.

Conflicts of Interest: The authors declare no conflicts of interest.

Abbreviations

The following abbreviations are used in this manuscript:

RCP	Rapid Control Prototyping
FNN	Feedforward Neural Network
PINN	Physics-Informed Neural Network
PDEs	Partial Differential Equations
PEHN	Physics-Embedded Hierarchical Network

References

1. Min Yu, Simos A. Evangelou, Daniele Dini. Advances in Active Suspension Systems for Road Vehicles. *Engineering*. **2024**, *33*, 160-177. https://doi.org/10.1016/j.eng.2023.06.014.
2. Xiaoqiang Sun, Chaochun Yuan, Yingfeng Cai, Shaohua Wang, Long Chen. Model predictive control of an air suspension system with damping multi-mode switching damper based on hybrid model. *Mechanical Systems and Signal Processing*,2017; 94, 94-110. https://doi.org/10.1016/j.eng.2023.06.014. https://doi.org/10.1016/j.ymssp.2017.02.033.
3. Sabrina Milani, Gabriele Marini, Giulio Panzani, Matteo Corno, Sergio M. Savaresi. Control-oriented modelling and experimental validation of a controllable multichamber air spring suspension. *Mechatronics*,2025; 112, 103406. https://doi.org/10.1016/j.mechatronics.2025.103406.
4. M.Y. Wu, H. Yin, X.B. Li, J.C. Lv, G.Q. Liang, Y.T. Wei, A new dynamic stiffness model with hysteresis of air springs based on thermodynamics, *Journal of Sound and Vibration*.2022;521: 116693. https://doi.org/10.1016/j.jsv.2021.116693.
5. Wu M, Hou J, Tong H, et al. A universal dynamical model of dual-chamber air springs with experimental validation. Proceedings of the Institution of Mechanical Engineers, *Part D: Journal of Automobile Engineering*. 2022;237(10-11):2553-2564. https://doi.org/10.1177/09544070221111645.
6. Li, Y.; Xiao, S.; Xie, J.; Zhu, T.; Zhang, J. Nonlinear Dynamic Mechanical Characteristics of Air Springs Based on a Fluid–Solid Coupling Simulation Method. *Appl. Sci. 2023, 13*, 12677. https://doi.org/10.3390/app132312677
7. Zhu, H., Yang, J., Zhang, Y. et al. Nonlinear dynamic model of air spring with a damper for vehicle ride comfort. *Nonlinear Dyn*.2017,89, 1545–1568. https://doi.org/10.1007/s11071-017-3535-9
8. Chen J-J, Huang Z-Q, Liu H-J, Qiu G-Q, Gu Y-K. A unified stiffness model of rolling lobe air spring with nonlinear structural parameters and air pressure dependence of rubber bellows. *Proceedings of the Institution*

of Mechanical Engineers, Part D: Journal of Automobile Engineering. 2024;239(2-3):407-431. 10.1177/09544070231214306

9. Zhao R, Xie H, Gong X, Sun X, Cao C. Neural Network-Based Adaptive Height Tracking Control of Active Air Suspension System with Magnetorheological Fluid Damper Subject to Uncertain Mass and Input Delay. *Sensors (Basel)*. 2023 Dec 27;24(1):156. https://doi.org/10.3390/s24010156.
10. Vijay Barethiye, G. Pohit, A. Mitra,A combined nonlinear and hysteresis model of shock absorber for quarter car simulation on the basis of experimental data,*Engineering Science and Technology, an International Journal*,2017,20;1610-1622. https://doi.org/10.1016/j.jestch.2017.12.003.
11. M. Raissi, P. Perdikaris, G.E. Karniadakis, Physics-informed neural networks: A deep learning framework for solving forward and inverse problems involving nonlinear partial differential equations, Journal of Computational Physics, 2019,378; 686-707, https://doi.org/10.1016/j.jcp.2018.10.045.
12. Cuomo, S., Di Cola, V.S., Giampaolo, F. et al. Scientific Machine Learning Through Physics–Informed Neural Networks: Where we are and What's Next. *J Sci Comput* 2022,**92**, 88 (2022). https://doi.org/10.1007/s10915-022-01939-z
13. Sifan Wang, Yujun Teng, Paris Perdikaris, Understanding and mitigating gradient pathologies in physics-informed neural networks. *SIAM Journal on Scientific Computing* 2021, 43(5), A3055-A3081. https://doi.org/10.1137/20M1318043.
14. Aditi Krishnapriyan, Amir Gholami, Shandian Zhe, Robert Kirby, Michael W. Mahoney, Characterizing possible failure modes in physics-informed neural networks. *Advances in Neural Information Processing Systems (NeurIPS)* 2021, 34, 26581-26592.
15. Ameya D. Jagtap, George Em Karniadakis, Extended physics-informed neural networks (XPINNs): A generalized space-time domain decomposition based deep learning framework for nonlinear partial differential equations. *Communications in Computational Physics* 2020, 28(5), 2002-2041. https://doi.org/10.4208/cicp.OA-2020-0164.
16. Karimi Eskandary, P., Khajepour, A., Wong, A. et al. Analysis and optimization of air suspension system with independent height and stiffness tuning. *Int.J Automot. Technol.* **17**, 807–816 (2016). https://doi.org/10.1007/s12239-016-0079-9.
17. Wu Qin, Xundong Liao, Ruqi Ding, Feifei Liu, Yiqian Zheng, Xiangnan Liu. Theoretical and experimental analysis of dynamic characteristics of a two-tube air spring with auxiliary reservoir. *Mechanical Systems and Signal Processing*.2025;233: 112764. https://doi.org/10.1016/j.ymssp.2025.112764.
18. Gao, Z.; Chen, S.; Zhao, Y.; Nan, J. Height Adjustment of Vehicles Based on a Static Equilibrium Position State Observation Algorithm. *Energies* **2018**, *11*, 455. https://doi.org/10.3390/en11020455
19. Pintado, P., Ramiro, C., Morales, A.L., Nieto, A.J., & Chicharro, J.M. The dynamic behavior of pneumatic vibration isolators. *Journal of Vibration and Control*, 2018;*24*, 4563 - 4574. 10.1177/1077546317730243
20. Hu, L.; Zhou, C.; Wan, Y.; Wang, H. Research on the Vibration Characteristics of Air Spring Suspension Seats Considering Friction Damping. *Appl. Sci.* **2025**, *15*, 5817. https://doi.org/10.3390/app15115817.
21. Wolf-Monheim, F., Schumacher, M., Frantzen, M. et al. Interlinked Air Suspension Systems. *ATZ Autotechnol* **9**, 58–61 (2009). https://doi.org/10.1007/BF03247122.
22. Hu, Y., Zhang, J. & Long, J. Influence of rubber's viscoelasticity and damping on vertical dynamic stiffness of air spring. *Sci Rep* 2023,**13**, 9886. https://doi.org/10.1038/s41598-023-36904-9.
23. Ji, H.; Lv, B.; Ding, H.; Yang, F.; Qi, A.; Wu, X.; Ni, J. Modeling and Control of Hysteresis Characteristics of Piezoelectric Micro-Positioning Platform Based on Duhem Model. *Actuators* **2022**, *11*, 122. https://doi.org/10.3390/act11050122.
24. Cao, X.; Wang, Q.; Xu, D.; Huang, S.; Wang, X.; Wang, L. Design and Analysis of Pneumatic Downforce Regulating Device for No-Till Corn Planter. *Agriculture* **2022**, *12*, 1513. https://doi.org/10.3390/agriculture12101513.
25. Zheng, Y.-T.; Wang, Z.-W. Response Analysis of a Vehicle–Cargo Coupling Model Considering Frequency-Dependent Characteristics of Air Suspension. *Appl. Sci.* **2025**, *15*, 8945. https://doi.org/10.3390/app15168945.
26. Korneyev, V.S., Korneyev, S.A. & Shalay, V.V. The improvement of scientific foundations for the technical theory of pneumatic elements with rubber-cord membranes: thermo-dynamic model of force and

 doi:10.20944/preprints202602.0491.v1

geometric characteristics of air springs. *J Mech Sci Technol* **38**, 49–65 (2024). https://doi.org/10.1007/s12206-023-1205-z.

27. Tuninetti, V.; Forcael, D.; Valenzuela, M.; Martínez, A.; Ávila, A.; Medina, C.; Pincheira, G.; Salas, A.; Oñate, A.; Duchêne, L. Assessing Feed-Forward Backpropagation Artificial Neural Networks for Strain-Rate-Sensitive Mechanical Modeling. *Materials* **2024**, *17*, 317. https://doi.org/10.3390/ma17020317.
28. Szekeres, B.J., Izsák, F. On the computation of the gradient in implicit neural networks. *J Supercomput* 2024,**80**, 17247–17268. https://doi.org/10.1007/s11227-024-06117-6.
29. Tuninetti, V.; Forcael, D.; Valenzuela, M.; Martínez, A.; Ávila, A.; Medina, C.; Pincheira, G.; Salas, A.; Oñate, A.; Duchêne, L. Assessing Feed-Forward Backpropagation Artificial Neural Networks for Strain-Rate-Sensitive Mechanical Modeling. *Materials* 2024, 17, 317. https://doi.org/10.3390/ma17020317.
30. Levi D. McClenny, Ulisses M. Braga-Neto, Self-adaptive physics-informed neural networks. *Journal of Computational Physics* 2023,29, 111722. https://doi.org/10.1016/j.jcp.2022.111722.
31. Karniadakis, G.E., Kevrekidis, I.G., Lu, L. et al. Physics-informed machine learning. *Nat Rev Phys* 2021,**3**, 422–440. https://doi.org/10.1038/s42254-021-00314-5.
32. Farea, A.; Yli-Harja, O.; Emmert-Streib, F. Understanding Physics-Informed Neural Networks: Techniques, Applications, Trends, and Challenges. *AI* **2024**, *5*, 1534-1557. https://doi.org/10.3390/ai5030074.
33. Sukirt Thakur, Maziar Raissi, Arezoo M. Ardekani, ViscoelasticNet: A physics informed neural network framework for stress discovery and model selection.*Journal of Non-Newtonian Fluid Mechanics*, 2024,330,105265. https://doi.org/10.1016/j.jnnfm.2024.105265
34. Arshia Merdasi, Saman Ebrahimi, Xiang Yang, Robert Kunz, Physics Informed Neural Network application on mixing and heat transfer in combined electroosmotic-pressure driven flow. *Chemical Engineering and Processing - Process Intensification* 2023,193,109540. https://doi.org/10.1016/j.cep.2023.109540.
35. Moritz Sprengholz, Christian Hühne, Zero-stiffness in rolling-lobe air springs for passive, load adaptable and low-frequency vibration isolation, *Journal of Sound and Vibration*, 2025, 608, 119061. https://doi.org/10.1016/j.jsv.2025.119061.
36. Hong, Y., Bansal, H. & Veroy, K. Physics-informed two-tier neural network for non-linear model order reduction. *Adv. Model. and Simul. in Eng. Sci.* 2024, **11**, 20. https://doi.org/10.1186/s40323-024-00273-3.